Springer

Journal of Mechanical Science and Technology 22 (2008) 2578~2589

Journal of Mechanical Science and Technology

www.springerlink.com/content/1738-494x
DOI 10.1007/s12206-008-0805-y

Influence of endplate on aerodynamic characteristics of low-aspect-ratio wing in ground effect †

Kyoungwoo Park[1] and Juhee Lee[2,*]

[1]*Mechanical Engineering, Hoseo University, Asan 336-795, Korea*
[2]*Department of Mechatronics Engineering, Hoseo University, Asan 336-795, Korea*

(Manuscript Received April 30, 2008; Revised June 10, 2008; Accepted August 4, 2008)

Abstract

A numerical analysis is performed to investigate the aerodynamic characteristics and static height stability of the endplate on aspect-ratio-one wing in ground effect. The investigation is carried out on angles of attack from 0^o to 10^o and ground clearances at a trailing edge from 5% of chord to 50%. The analysis shows that the ground effect increases the lift by high pressure on the lower surface, reduces the induced drag, increases the suction on the upper surface, and consequently considerably enhances the lift-drag ratio. The endplate, which prevents the high-pressure air escaping from the air cushion and reduces the influence of wing-tip vortex, augments lift and lift-drag ratio further. Interestingly, the drag with the endplate does not increase as much as the lift does when the airfoil is brought close to the ground. From the analysis and visualization of computation results with the endplate, it is found that two wing-tip vortices are generated from each wing surface, their strengths are stronger, diminished rapidly and the influence of the wing-tip vortices are decreased. The outward drift of wing-tip vortex, which is generated from the lower wing surface, is observed. Irodov's criteria are also numerically evaluated to investigate the static height stability of wings with and without the endplate. The comparison of Irodov's criteria shows that the endplate is not favorable for static height stability but reduces the deviation of the static height stability with respect to pitch angles and heights.

Keywords: WIG vehicle; Ground effect; Endplate; Low-aspect-ratio wing; Aerodynamic characteristics

1. Introduction

According to the globalization and information technology of industries, transportation has become a center of key industries for the last decade. The von Karman-Gabriell's diagram [1] depicts the efficiency of various transportations. A remarkable thing in the diagram is the triangular area at the center of the technology line where no conventional means of transportation appears. The WIG (wing-in-ground effect) craft, a flying ship cruising with the speed of 100 to 400 km/h and a lift-to-drag ratio of 15 to 30, can fill the speed and efficiency gap between marine and air transports. In general, the lift and drag forces of a wing will considerably change near the ground. These phenomena during the takeoff and landing have been observed by many researches [2-5] from early 1900s. According to their results, the ground has a great influence (suction and stagnation) on pressure distribution along the wing surface. Incoming air to the lower wing surface gradually decreases the magnitude of the speed and changes dynamic pressure to static pressure. This eventual increase of pressure is called an air cushion.

Wieselsberger [2] in his theoretical study insisted that a longer runway for landing was necessary because of an excessive lift force due to this air cushion. Pressure distributions on the lower surface become somewhat constant and the strength of the pressure increases with the ground proximity by air cushion.

† This paper was recommended for publication in revised form by Associate Editor Haecheon Choi
*Corresponding author. Tel.: +82 41 540 9669, Fax.: +82 41 540 5808
E-mail address: juheelee@hoseo.edu

On the other hand, the pressure distributions on the upper surface depend on the suction by the wing profile. In general, the pressure rise on the lower surface is considerably high when the wing is in the ground effect and the resultant forces of the pressure lead an increase in the lift forces. By constant pressure distributions on the lower surface, the center of the pitching moment tends to move to the mid chord where it is behind the center of gravity. The stability of the wings in ground effect is also changed according to the center of the pitching moment. For a finite wing in ground effect, the induced drag is decreased because of the decreased influence of the wing tip vortex while the strength of the wing-tip vortex is increased. Joh and Kim [6] compared the total pressures of the vortex core for IGE (in ground effect, h/c=0.3) and OGE (out of ground effect) cases and they found that the vortex strength was growing with the ground proximity, whereas the induced drag was reduced. Wieselsberger [2] performed a theoretical investigation of the ground effect to determine the conditions in taking off and landing of an airplane with Prandtl's wing theory. He utilized the principle of reflection and replaced the surface of the ground by the second wing at the same distance but on the opposite side. The reduction in induced drag of a monoplane and multi-plane in ground effect was estimated in terms of the ground influence coefficient, aspect ratio, and lift coefficient. His predictions were in good agreement with experimental results.

Ahmed et al. [5] and Hsiun and Chen [7] predicted the flow characteristics of NACA 4412 by experiment and numerical method respectively. A sudden increase of the lift coefficient was observed as the ground was approaching because a stationary wall boundary was used. This increase did not happen in a real flight. Both investigations found the increase of the suction on the upper surface and increase of the pressure on the lower surface in two-dimensional flow. For the zero-degree angle of attack ($\alpha = 0^o$), the lift force was almost zero at ***h/c*** = 0.05 due to the strong suction effect on the lower surface and the laminar separation. The endplate prevents the flow exiting through the wing tip instead of the small gap at the trailing edge and ultimately increases the ground effect exerted on the wing surface. Recently developed WIG crafts are generally equipped with an endplate to improve the aerodynamic performance. However, the aerodynamic characteristics on the endplate have not been fully investigated in both experimental and/or numerical researches until now. Only few experimental investigations on the effect of endplate were performed by Fink and Lastinger. [3] and Carter [4]. Fink and Lastinger [3] performed a series of wind-tunnel investigations to determine the ground effect on the aerodynamic characteristics of thick and highly cambered wings with various aspect ratios. They used the two wings on opposite sides of the imaginary ground. All wings in the experiments increased the lift slope and reduced the induced drag, which resulted in the increase of lift-drag ratio. Due to constant pressure distributions on the lower surface, they predicted an increase in static longitudinal stability at positive angles of attack but a decrease at negative ones. They also observed a reduction in induced drag with no change in wing profile as the wing approached the ground. The effect of the endplate, which was extended one-inch below and parallel to the lower surface of the wing, was briefly mentioned in the study. According to their investigation, an endplate showed the effect of preventing the stagnated air on lower surface from flowing out around the wing tips and produced a substantial improvement in lift-drag ratio. On the other hand, the ground had no effect on the maximum lift of the plane wings but reduced the maximum lift coefficient of the wings equipped with split or slotted flaps [8].

Many numerical and experimental studies have been performed to predict the aerodynamic characteristics of wing in the ground effect. However, much less study has been devoted to analyzing the flow field around an endplate which has an aspect ratio (AR) of one. To the authors' knowledge, a detailed aerodynamic analysis on the influence of the endplate in WIG craft has not been reported. Therefore, in the present work, the influence of the endplate on the aerodynamic characteristics of a rectangular wing in ground effect in viscous flow is studied numerically. Numerical analyses are performed by solving the Reynolds averaged Navier-Stokes (RANS) of turbulent flow, and the aerodynamic characteristics (i.e., lift, lift-to-drag ratio, pressure distribution and static height stability) are compared for the case of with and without endplate for various conditions such as angle of attack (α) and non-dimensional height (***h/c***).

2. Geometry parameterization and CFD model validation

2.1 Numerical methods

The physical configuration of the endplate considered in this study is presented in Fig. 1. Air is taken as the fluid and is assumed to be steady, incompressible and turbulent. The shape of the endplate is three-dimensional. The fluid properties are taken to be constant and the effect of viscous dissipation is assumed to be negligibly small. Using the aforementioned assumptions, the Reynolds-Averaged Navier-Stokes (RANS) equations for mass and momentum, which are written in a tensor notation, have to be solved.

$$\frac{\partial(\rho u_j)}{\partial x_j} = 0 \tag{1}$$

$$\frac{\partial(\rho u_i u_j)}{\partial x_j} = -\frac{\partial P}{\partial x_i} + \frac{\partial}{\partial x_j}\left[\mu\left(\frac{\partial u_i}{\partial x_j} + \frac{\partial u_j}{\partial u_i}\right) - \overline{\rho u_i' u_j'}\right] \tag{2}$$

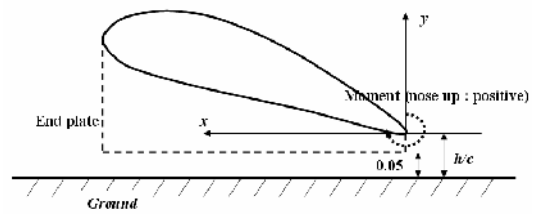

(a) 2-dimensional view

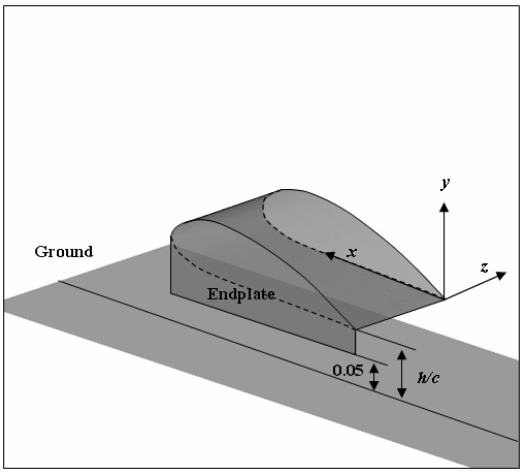

(b) 3-dimensional view

Fig. 1. Physical model of wing in ground effect.

The new term, $\overline{\rho u_i' u_j'}$, the Reynolds stress, must be modeled by using a turbulence model in order to solve the RANS equations. In this study, the flow domain was divided into two regions, such as near wall and fully turbulent regions, and then we adopted a standard turbulent model [9] and wall function next to the wall. According to this model, turbulent kinetic energy (***k***) and its dissipation rate (ε) are expressed in a tensor form as follows:

$$\frac{\partial}{\partial x_j}(\rho u_i k) = \frac{\partial}{\partial x_j}\left[\frac{\mu_t}{\sigma_k}\frac{\partial k}{\partial x_j}\right] + P_k - \rho\varepsilon \tag{3}$$

$$\varepsilon = \frac{k^{3/2}}{l_\varepsilon}\left(1 + \frac{C_\varepsilon}{\mathrm{Re}_y}\right) \tag{4}$$

where ***i*** = 1, 2 and 3 denote x, y, and z directions, respectively. The term P_k in Eq. (3) stands for the production term. The model constants and various functions used in the turbulent model are detailed in reference [9].

The numerical simulations presented in this work were done by means of STAR-CD [10], which is a general purpose commercial software. The pressure-velocity coupling phenomenon is resolved through the SIMPLE algorithm [11]. For representing the exact flight conditions, the moving wall boundary condition with a flight velocity is applied at the ground. The solutions are treated as converged ones when the sum of residual is less than 1×10^{-7}.

2.2 Validation of CFD model and grids

The numerical results for modified Glenn Martine 21 airfoil at two different computational conditions, ***h/c*** = 0.176 and 2, are obtained by the present method and compared with the experimental data [3]. Computations are performed at $\alpha = 0^o$ with the aspect ratio of one and Reynolds number of 0.46×10^6. Endplates are not attached in these validation cases. The modified Glenn Martine 21 airfoil listed in Table 1 is modified to provide a flat-bottom wing from the 30% of the chord to the trailing edge. Figs. 2 and 3 show the comparisons of lift coefficient and drag polar, respectively, at ***h/c*** = 0.176 and 2 and show good agreement with the experiments. The experiments were conducted by the image-wing method [3] since this method did not present the boundary-layer problems between the wing and ground. The wings in Fig. 2(a) and (b) are sufficiently close to the ground and

Table 1. Modified airfoil section of Glenn Martin 21.

x/c	Airfoil ordinates (y/c)	
	Upper	Lower
0.000	0.0886	0.0860
0.0125	0.1221	0.0603
0.025	0.1381	0.0479
0.050	0.1598	0.0333
0.075	0.1765	0.0235
0.100	0.1892	0.0172
0.150	0.2072	0.0075
0.200	0.2168	0.0028
0.300	0.2213	0
0.400	0.2113	0
0.500	0.1920	0
0.600	0.1664	0
0.700	0.1335	0
0.800	0.0943	0
0.900	0.0500	0
0.950	0.0257	0
1.000	0	0

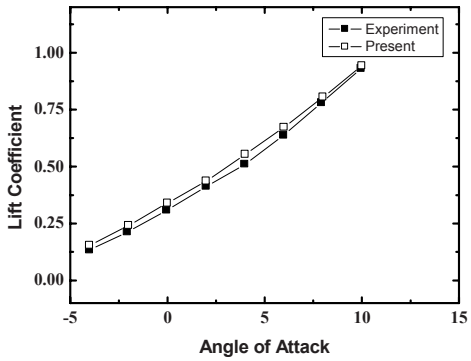

(a) Lift coefficient vs. angle of attack at h/c=0.176

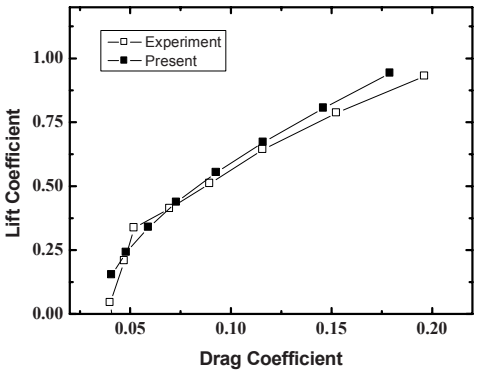

(b) Drag Polar at h/c=0.176

Fig. 2. Comparison of aerodynamic characteristics in ground effect (IGE).

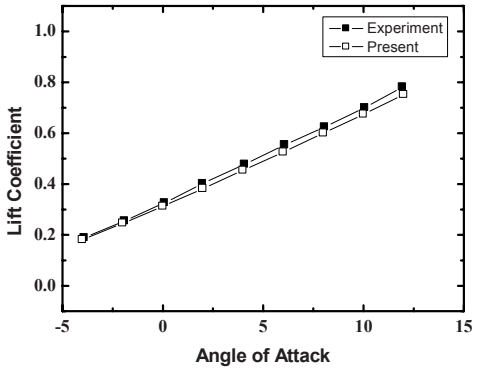

(a) Lift coefficient vs. angle of attack at ***h/c***=2

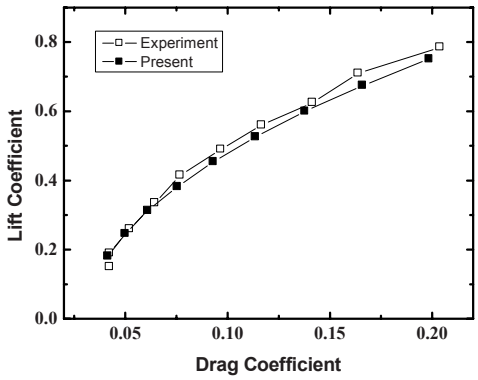

(b) Drag Polar at ***h/c***=2

Fig. 3. Comparison of aerodynamic characteristics out of ground effect (OGE).

are in ground effect (IGE), while the wings in Fig. 3(a) and (b) are far away from the ground and are out of ground effect (OGE). The RNG k-ε model is used for predicting the turbulent flow and the near-wall flow is computed by using a wall function. Due to the geometric symmetry conditions of the model, only half of the model is simulated. Five layers of the prism mesh are used to resolve the boundary layer on the wing surface and $y^+_{\max}$ values are about 50 over the wing surface.

3. Results and discussion

A computational analysis around the finite wing is performed with the same grids and numerical schemes as discussed in the preceding chapter. The computational domain used in this study is extended 10 times of a chord for each direction to avoid the influence of the far boundaries but 30 times for downstream. To take the wake behind the wing into

account correctly, dense grids as well as prism meshes are used in the extended area of 4 times of a chord. Five layers of the prism mesh are adopted to predict the accurate flow near wing and endplate and grid system is shown in Fig. 4. In this study, the y^+_{max} values on the ground and on the wing surface are estimated as less than 20 and 50, respectively. Non-dimensional height, ***h/c***, between the wing and ground is measured at the trailing edge and a nose-up pitching moment is positive as seen in Fig. 1. As shown in Fig. 1(b), the downward endplate is placed at the wing tip and the bottom edge of an endplate is parallel to the ground surface. The distance between endplate and ground remains constant irrespective of the height and angle of attack in order to predict the aerodynamic performance for the cruise condition. The numerical calculation with the endplate is restricted from ***h/c*** = 0.1 to 0.3 because of the constant height of the endplate from ground and length of the endplate which is virtually too long at ***h/c*** = 0.5.

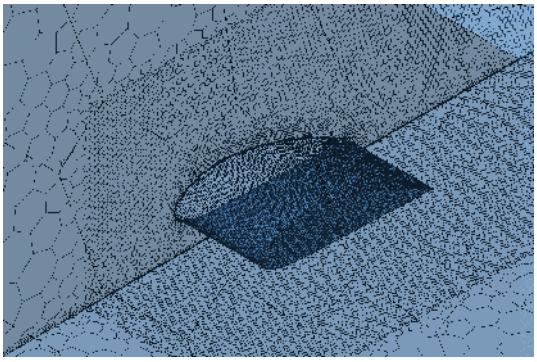

(a) Polyhedral meshes and prism layers on the wing and ground

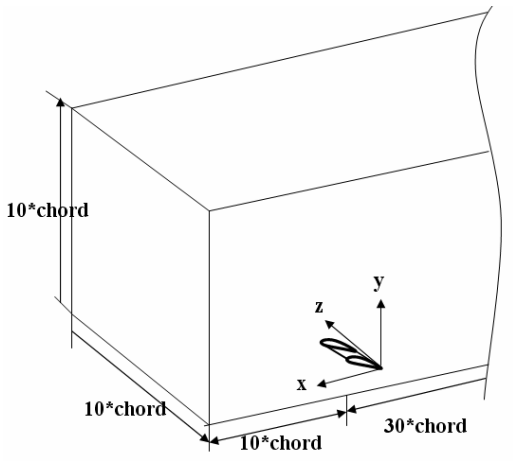

(b) Computational domain and wing

Fig. 4. Grid systems and Computational domain.

In order to explain the effect of endplate on the lift force according to the airfoil height (***h/c***), the lift coefficients for various values of α ($0^o \sim 10^o$) are displayed in Figs. 5 and 6. Fig. 5 shows the results for without endplate and for the case of with endplate are shown in Fig. 6. It is found that the proximity to the ground results in an increase of the lift force for all angles of attack except $\alpha = 0$. Generally, lift coefficients with reduced heights mainly depend on the shape of the passage between the wing and the ground. For instance, a symmetric airfoil without a camber or an airfoil with a moderate camber recorded lower values of lift force with ground proximity because of its divergent-convergent passage or thickness effect as reported by References [7] and [6]. Ahmed and Sharma [12] showed different results in their experiment with a symmetric airfoil of NACA0015. The difference is caused by both the blockage effect and the non-slip ground plate since the airfoil almost contacts the ground plate at ***h/c*** = 0.1, which is measured from the ground to the trailing edge. A modified Glenn Martin 21 airfoil for the WIG craft used in this study has geometrical advantage and reduces the deep decrease of lift by thickness effect at low angles of attack somewhat as shown in Fig. 5(a). The same results as this study can be found in the study of Ahmed and Goonaratne [13]. This study on the same wing profile, different low-aspect ratios and a different endplate showed that the wing could provide lift augmentation when they were in the influence of the ground effect. They reported that the lift for the thick and flat-bottom airfoil (i.e., cambered airfoil) was increased as the angle of attack increased and the height decreased. For $\alpha = 0^o$ in Fig. 5, the values of lift are not changed except the very close to the ground, but the values of lift exponentially increase at ***h/c*** < 0.3 and $\alpha = 2 \sim 8^o$. Thus, these increases in lift at the lower height lead the wing back to its original height when the wing decreases its height somewhat. It is possible to say that the Glenn Martin 21 wing profile without an endplate is therefore stable in height at positive angles of attack. Interestingly, the lift force at $\alpha = 0^o$ is almost constant at ***h/c*** > 0.1. On the other hand, it can be seen in Fig. 6 that the existence of endplate captures the increase of lift force compared with the case without endplate for all conditions because of higher pressures under the airfoil. That is, the endplate brings on the increase in lift

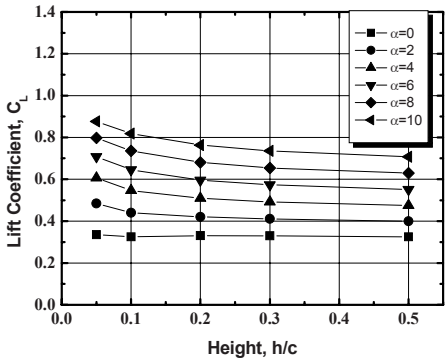

(a) Lift coefficient with respect to height

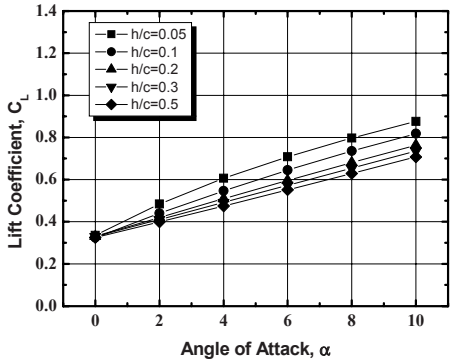

(b) Lift coefficient with respect to angle of attack

Fig. 5. Lift coefficient without endplate.

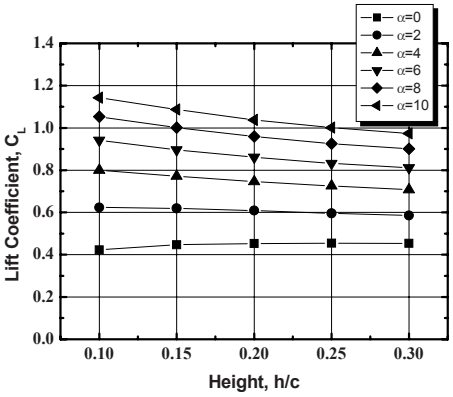

(a) Lift coefficient with respect to height

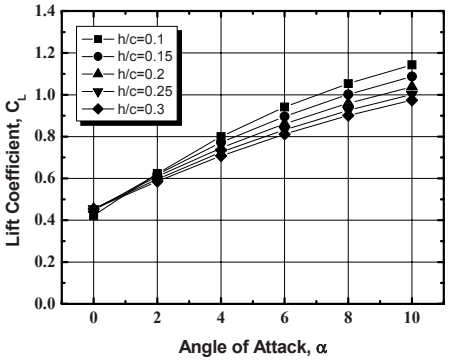

(b) Lift coefficient with respect to angle of attack

Fig. 6. Lift Coefficient with endplate.

force at the same angle (α) and height (***h/c***). However, the values of lift forces in Fig. 6(a) are virtually decreased with reduced height at $\alpha = 0^o$. The decrease in lift at low angles, which is observed in some researches [3, 5, 6], is caused by the thickness effect. In general, the lift force of the wing in ground effect depends on three facts: the suction on the upper surface, the divergent-convergent passage on the lower surface and the pressure augmentation on the lower surface. Only the divergent-convergent passage or thickness effect is not favorable for lift. Decrease of lift at $\alpha = 0^o$ by this thickness effect can apparently be seen in Fig. 6(b). Interestingly, the slight decrease also can be seen in Fig. 5(a) at $\alpha = 0^o$ and ***h/c*** =0.1. The decrease of lift forces also comes from the thickness effect. An interesting result can be seen in Fig. 5(b) that the lift is increased with the angle of attack nonlinearly when the wing is sufficiently close to the ground such as ***h/c*** $\leq$ 0.1. The same increment for all heights can be observed in Fig. 6(b). The facts suggest that the influence of the ground effect with endplate reaches higher than without endplate. The drag coefficient for different values of α and ***h/c*** is shown in Fig. 7. For ***h/c*** $\geq$0.5 (not plotted), the wings are, indeed, completely out of ground effect and the significant changes of lift and drag were not observed. However, for ***h/c*** <0.3, because the wings begin to affect the ground effect, the drag forces change nonlinearly for both cases. The drag force can be decomposed into its pressure drag, induced drag, and friction drag nominally. The skin friction from the computational result is constant with respect to height but is slightly variable with respect to α . Consequently, the contribution of the skin friction to total drag can be ignored for the analysis. When the wing is sufficiently close to the ground and at low angles of attack, the effect of pressure drag to total drag is relatively small because of its direction, but the effect of

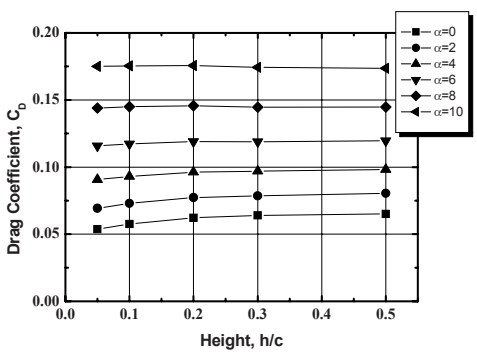

(a) Drag coefficient without endplate

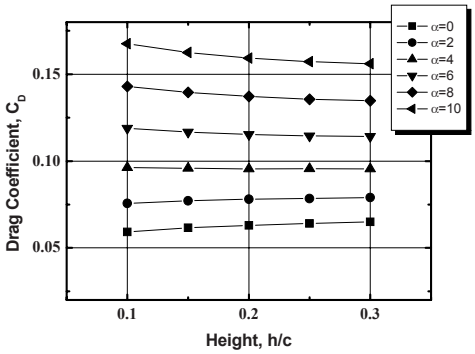

(b) Drag coefficient with endplate

Fig. 7. Drag coefficient with respect to height.

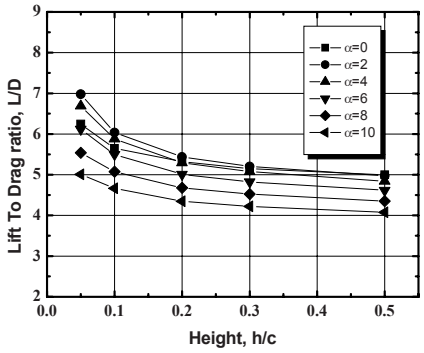

(a) Lift-drag ratio without endplate

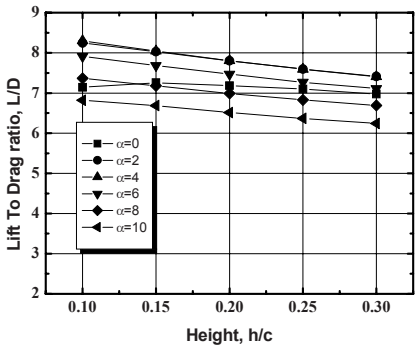

(b) Lift-drag ratio with endplate

Fig. 8. Lift-drag ratio with respect to height.

induced drag is not. However, the influence of the two drags may be in balance at higher angle of attack and drag coefficient can be constant as shown in Fig. 7. A constant drag with respect to height is recorded at $\alpha = 8^o$ in Fig. 7(a) and $\alpha = 4^o$ in Fig. 7(b). The increase of drag can be seen after the constant-drag line at $\alpha = 4^o$ with reducing ***h/c*** in Fig. 7(b). Many studies also show constant drag in their study. Even though the results cannot be compared directly because of the different definition of height, which is defined at quarter chord, Fink and Lastinger [3] also observed constant drag at $\alpha = 6^o$. Ahmed and Goonaratne [13] performed the experiment with low-aspect-ratio wing and noted that the drag coefficient remains constant with increasing ground clearance for a particular flap angle. Ahmed and Sharma., [12] observed that the drag coefficient increased slightly with ground clearance. In 2-dimensional analysis [7], the drag also decreases with the decreasing height because of the change of pressure drag of the airfoil in ground effect. The theoretical treatment of ground effect presented by Wieselsberger [2] showed the reduction of induced drag for a wing with decreased height. Fig. 8 depicts the lift-drag ratio of the results. It can be clearly seen in Fig. 8 that the wing with the endplate has larger value of the lift-drag ratios than that of without the endplate. The lift-drag ratios in Fig. 8(a) exponentially increase with decreasing height, while Fig. 8(b) shows that the lift-drag ratios linearly increase. The maximum lift-drag ratios for the case with and without endplate are recorded at $\alpha = 2^o$ and $\alpha = 4^o$ respectively. The endplate improves the lift-drag ratio due to increase in lift by air cushioning on the lower wing surface and a decrease in induced drag. Steep decreases of lift-drag ratio with endplate are observed at $\alpha = 0^o$ by a decrease in the lift because of the thickness effect as shown in Fig. 6(b). Raymond [14] carried out experiments for the three different airfoils--Martin No.2, R.A.F 15 special and U.S.A. 27--and showed that the lift-drag ratio with

respect to height was lessened at high α. Fink and Lastinger [3] with the same wing profile, modified Glenn Martin 21, also showed the maximum lift-drag ratio at $\alpha = 4^o$. The results were not directly compared because of the different definition of height which was measured at the quarter chord. The aerodynamic forces of wing in ground effect, which are affected by changes of α as well as ***h/c***, lead to a different stable condition from out of ground effect. The static height stability (HS), a condition for the wing in ground effect considering both α and ***h/c***, was proposed by Irodov [15] and is plotted in Fig. 9.

Irodov derived HS with a coordinate system that has an origin at a trailing edge. In this study, the same coordinate system was used for convenience. The calculation of the static height stability condition includes the differentiations of lift coefficient and pitching moment coefficient against heights and angles of attack. To avoid numerical errors and excessive calculations, the differentiations are evaluated from the interpolation functions of lift coefficient and pitching moment instead of the direct numerical differentiations. Although an interpolation function is used, proper values of differentiation at $\alpha = 0^o$ cannot be obtained because of the sudden increase of numerical errors by small changes of values. So the comparison of HS at $\alpha = 0^o$ is ruled out in Fig. 9. Two different functions, second-order polynomial for the lift coefficient and double exponential functions [6] for the moment coefficient, are employed:

$$C_L = C_{L0} + A_1\alpha + A_2\alpha^2 \tag{5}$$

$$C_M = C_{M0} + B_1 e^{h/Chord/t_1} + B_2 e^{h/Chord/t_2} \tag{6}$$

where $C_{L0}, A_1, A_2, C_{M0}, B_1, t_1, B_2,$ and t_2 are independent variables for the curve regression.

$$HS = \frac{C_{M,\alpha}}{C_{L,\alpha}} - \frac{C_{M,h}}{C_{L,h}} = X_\alpha - X_h \le 0 \tag{7}$$

where h and α in the moment coefficient and the lift coefficient represent the derivative of the height and the angle of attack, respectively. The pitching moments are measured at a trailing edge. One might expect that the simplest condition for the static height stability is:

$$C_{L,h} < 0 \tag{8}$$

For stability, when the increase of the height will indeed lead to the decrease of the lift, it apparently satisfies the stable condition. The fact that the moment coefficient changes due to the height is not, however, taken into account in Eq. (8). So the equation is only valid when the wing is in a trimmed condition; in other words, C_M must be held constant. Eq. (7) takes into consideration the actual conditions: lift and moment according to α and ***h/c***. As shown in Eq. (7), HS implies the distance between two neutral points, X_h for neutral point of heights (***h/c***) and X_α for the neutral point of angles (α). The positive direction of X, a distance measured from the trailing edge, is upstream. Consequently, HS condition can be satisfied, if X_h is upstream of X_α. Fig. 9 apparently shows decreases of HS with respect to ***h/c*** at the low angles ($\alpha = 2^o$ and 4^o) and increases at the high angles ($\alpha = 6^o \sim 10^o$). These changes mainly come from X_h. Changes of the X_α against heights and angles of attack are moderate and linearly decrease as the height decreases. It implies that lift and

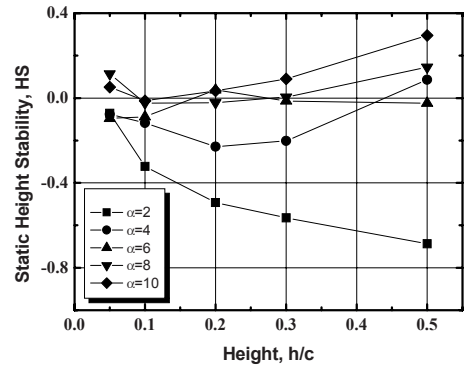

(a) Static height stability without endplate

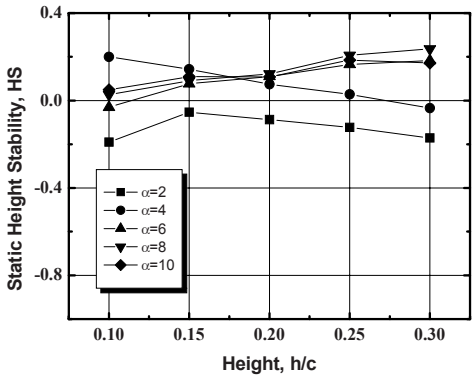

(b) Static height stability with endplate

Fig. 9. Static height stability with respect to height.

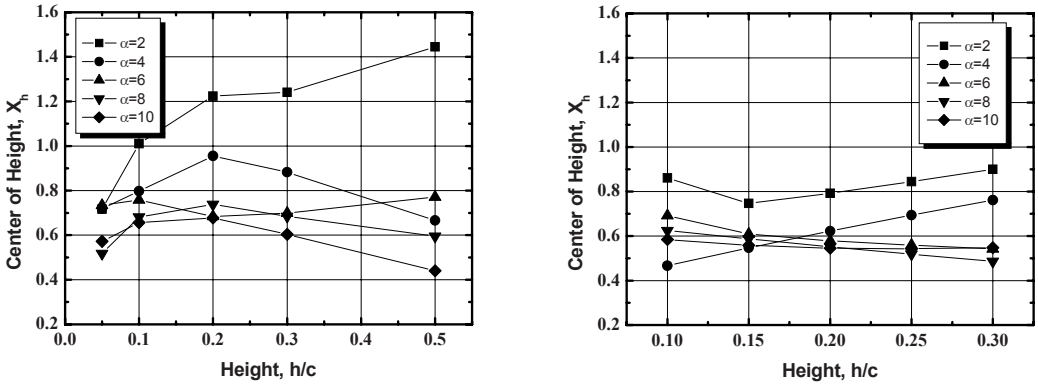

(a) Center of height without endplate (b) Center of height with endplate

Fig. 10. Aerodynamic center of height with respect to height.

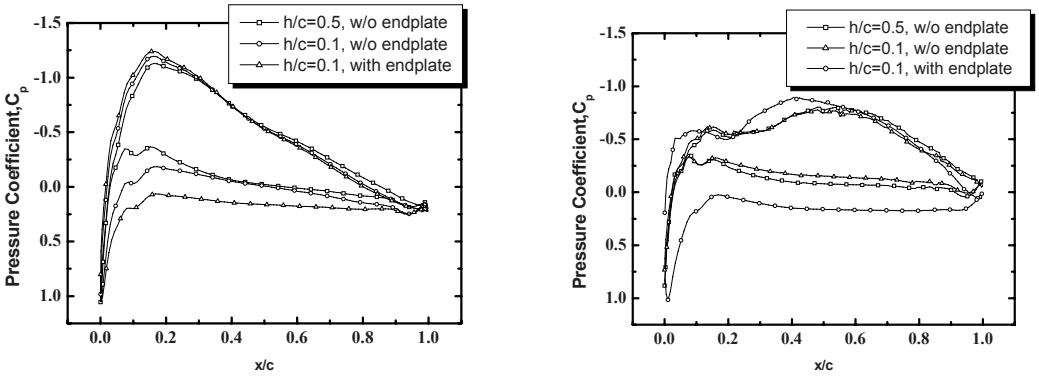

(a) Pressure distributions at z/Span=0 (b) Pressure distributions at z/Span=0.9

Fig. 11. Effect of the height and endplate on pressure coefficient at $\alpha = 2^o$.

pitching moment are linearly increased as angle of attack and the rate was not changed much except the wing extremely close to the ground. The condition of HS for the case with the endplate is only satisfied at $\alpha = 2^o$. As a result, the endplate is not favorable for HS since X_h for the case with endplate moves to around ***h/c***=0.6 while the X_h moves to at around ***h/c***=0.7 for without endplate as shown in Fig. 10. Comparing Fig. 9(a) and (b), the deviation of HS for with endplate is, however, smaller than that for without endplate. The small deviation makes the cruise control easy. There is a practical condition for static height stability in Reference [16]; the center of gravity should be located between X_h and X_α . X_h for without endplate, which is placed near to the quarter chord, is more favorable. In Fig. 11, the pressure distributions on the wing surface show the effect of the ground and the endplate in detail. For the cases of ground effect and endplate, a considerable increase and decrease in pressure are found on the lower surface and the upper surface, respectively. The air, which tends to stagnate under the airfoil due to the ground effect, causes a reduction in velocity and an increase in pressure on the lower surface. The suction on the upper surface increases due to divergence of the flow towards the upper surface. Moreover, the endplate prevents the flow exiting through the wing tip instead of the small clearance at the trailing edge, and consequently helps to augment the lift further. A higher pressure on the lower surface by stagnation is also observed in studies on NACA 4412 [5, 7], but lower pressure on the upper surface is not. A modified Glenn Martin 21 airfoil used in this study has divergence of the flow toward the upper surface and improves the lift further. In Fig. 11(b) at the wing tip, circular symbols show the significantly lower pressures on the lower surface, which have the same magnitude as that at mid-span in Fig. 11(a). The end-

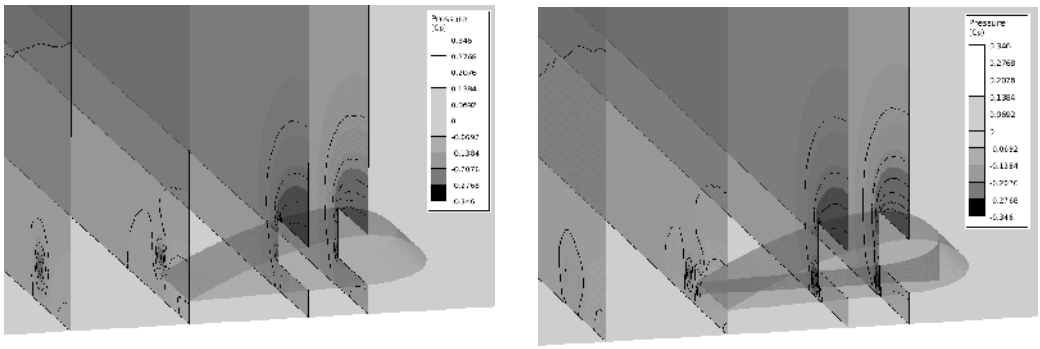

(a) Pressure distribution without endplate (b) Pressure distribution with endplate

Fig. 12. Effect of endplate on pressure distribution at ***x/c***=0.5, 0.75, 1, 1.5 from leading edge at ***h/c***=0.1.

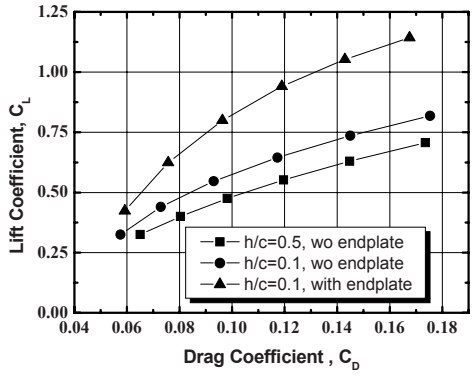

Fig. 13. Drag Polar at $h/c = 0.1$.

plate, which prevents air exit, keeps a high pressure on the lower surface until the wing tip. The wiggles on the upper surface imply the existence of the wing-tip vortex at that point. To explain the effect of endplate on the flow structures clearly, the pressure distributions at ***x/c***=0.5, 0.75, 1.0 and 1.5 are displayed for with and without endplate in Fig. 12. It can be easily seen that the endplate changes pressure distributions and it augments the strength of the pressure on the entire lower surface. Additionally, the endplate makes the pressure distributions on the lower to be constant. Fig. 12(b), which is indicated the influence of the endplate, shows that the lowest pressure is occurring near the endplate at ***x/c***=0.5 and then the strength of pressure is rapidly diminished after a trailing edge. In Fig. 13, an improvement in the aerodynamic performance for the case of the endplate is apparently shown. It is interesting to speculate about the reduction of drag force by the ground and the endplate on these results. In Fig. 13, the rapid increase in drag for the circular symbol, which is the case of without endplate at ***x/c***=0.1, is observed with an increasing lift because of the contribution of the high pressure drag. However, the contribution of the pressure drag with endplate is not significant as much as that without endplate. As a result, total drag for with endplate keeps its lower values until the higher lift. The contour and iso-surfaces of strength of vorticity are able to visualize the growth of the wing-tip vortices as shown in Figs. 14 and 15, respectively. Two wing-tip vortices are generated from each side at the mid-chord, flow downstream and are growing. The strength of the vorticity for the endplate is much stronger and the center of the vortex is pushed outward from the wing tip as shown in Fig. 14(b). At the trailing edge, ***x/c***=1.0, the two wing-tip vortices, which are not merged to one, are clearly observed in Fig. 14(b) and rapidly diminished along downstream. The plot of the iso-surface in Fig. 15(b) apparently shows the two wing-tip vortices which are not merged. From Figs. 14 and 15, it is concluded that when the endplate is equipped to the wing in ground effect, a jet-like flow tends to push the wing-tip vortex at the lower surface. The distance between two separated wing-tip vortices is too great to merge at the trailing edge. It is expected that the influence of the wing-tip vortex is considerably reduced.

4. Conclusions

This work analyzed the aerodynamic characteristics around the airfoil (lift force, lift-to-drag ratio, pressure distribution and height stability) numerically in order to predict the effect of the endplate. The endplate extending downward at the wing tip prevents escaping high-pressure air from under the wing and maxi-

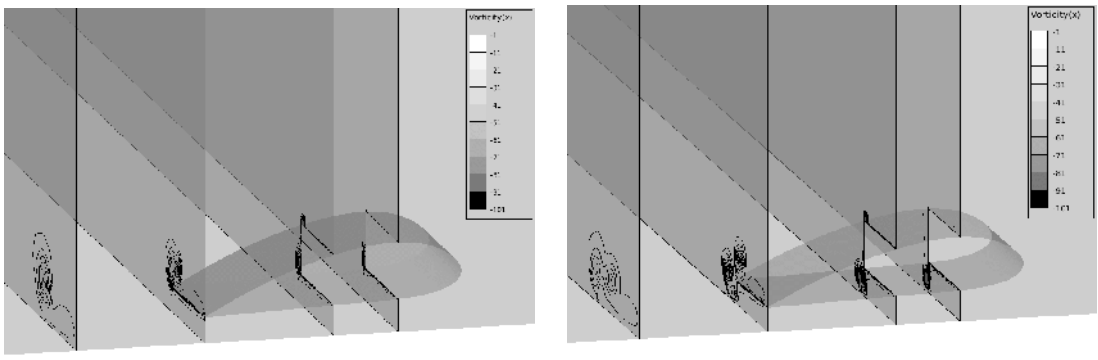

(a) Vorticity strength without endplate (b) Vorticity strength with endplate

Fig. 14. Effect of endplate on vorticity strength at ***x/c***=0.5, 0.75, 1, 1.5 from leading edge at ***h/c***=0.1.

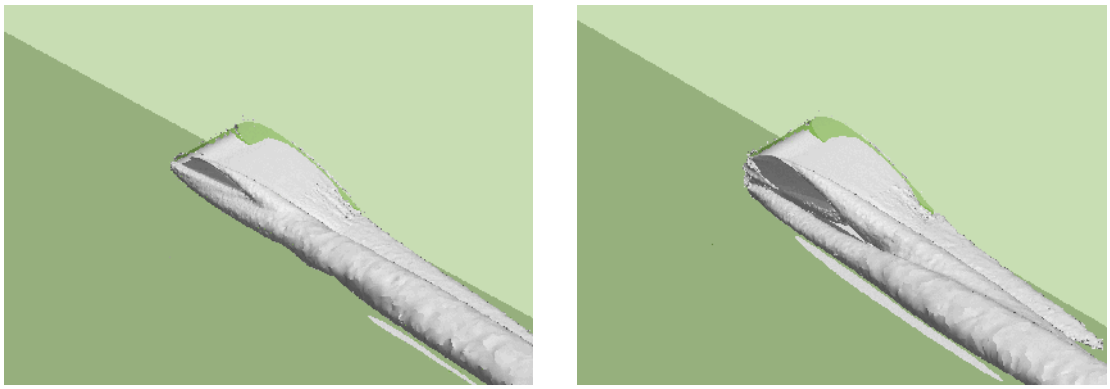

(a) Iso-surface of vorticity strength without endplate (b) Iso-surface of vorticity strength with endplate

Fig. 15. Effect of endplate on vorticity strength.

mizes the ground effect while the drag force remains constant or slightly increases only. Unlike wings out of ground effect, the air flows to the wing tip, and the wing-tip vortex generated under the wing surface is pushed away from the wing tip. The wing in ground effect increases the lift and decreases the drag as it approaches the ground. The endplate also increases lift and lift-drag ratio further. The wing without an endplate at $\alpha = 6 \sim 10^o$ and with an endplate at $\alpha = 4 \sim 10^o$ does not satisfy the static height stability, HS. It is found that the stability is mainly affected by the X_h rather than X_α which linearly decreases as the height is decreased. Briefly, X_α moves upstream while X_h moves downstream at low α but upstream at high α. Moving X_h upstream is favorable for the static height stability. Interestingly, because of the suction at $\alpha = 0$, the lift-drag rapidly decreases for both the cases, with and without endplate, because of decrease in lift. On the other hand, the wing-tip vortex for the endplate is separated into two and has been diminished rapidly along downstream. This may be one of the significant reasons for decreasing induced drag for a wing with endplate. The endplate captures the high-pressure air under the wing and increases the lift and lift-drag ratio further. From the visualization of computation results, two wing-tip vortices are generated from each surface of the wing tip, and their strength is weak and diminishes rapidly. The endplate can improve the aerodynamic characteristics in ground effect.

Acknowledgments

This work was supported by grant No. RTI04-01-02 from the Regional Technology Innovation Program of the Ministry of Commerce, Industry and Energy (MOCIE).

Nomenclature

AR : Aspect ratio (b^2/S)

b : Span
c : Chord length
C_D : Drag coefficient ($D/0.5\rho_\infty v_\infty^2 S$)
C_L : Lift coefficient ($L/0.5\rho_\infty v_\infty^2 S$)
C_M : Moment coefficient ($M/0.5\rho_\infty v_\infty^2 SC$)
C_ε , l_ε : Empirical constants for turbulence model
D : Drag
h : Height at trailing edge or at quarter chord
HS : Static height stability, Eq. 7
k : Turbulent kinetic energy
L : Lift
M : Pitching moment
Re_y : Reynolds number based on y direction
S : Wing area
v_∞ : Free stream velocity
u_i , u_j : Velocity component
$y^+_{\max}$: Maximum value of shear Reynolds number

Greeks

α : Angle of attack, pitching angle
ε : Dissipation rate of k
μ_t : Turbulent viscosity

References

[1] http://www.se-technology.com.
[2] C. Wieselsberger, Wing resistance near the ground, NACA TM No. 77, (1922).
[3] M. P. Fink and J. L. Lastinger, Aerodynamic characteristics of low-aspect-ratio wings in close proximity to the ground, NASA TN D-926 (1961).
[4] A. W. Carter, Effect of ground proximity on the aerodynamic characteristics of aspect-ratio-1 airfoils with and without end plate, NASA TN D-970 (1961).
[5] M. R. Ahmed, T. Takasaki and Y. Kohama, Aerodynamics of a NACA4412 airfoil in ground effect, *AIAA Journal*, 45 (1) (2007) 37-47.
[6] Chang-Yeol Joh and Yang-Joon Kim, Computational aerodynamic analysis of airfoil for WIG (Wing-In-Ground-Effect) – craft, *JSAS*, 32 (8) (Korean), (2004) 37-46.
[7] C. Hsiun and C. Chen, Aerodynamic characteristics of a two-dimensional airfoil with ground effect, *J. of Aircraft*, 33 (2) (1996) 386-392.
[8] I. G. Recant, Wing-tunnel investigation of ground effect on wing with flaps, NACA TN No. 705 (1939).
[9] W. Rodi, *Turbulence models and their applications in hydraulics-a state art of review*, Book Publication of International Association for Hydraulic Research, Delft, Netherlands, (1984).
[10] STAR-CD v4.00, Methodology, Computational Dynamics, Co., London. U. K, (2006).
[11] S.V. Patankar, *Numerical Heat Transfer and Fluid Flow*, McGraw-Hill Book Company, New York, (1980).
[12] M. R. Ahmed and S. D. Sharma, An investigation on the aerodynamics of a symmetrical airfoil in ground effect, *Experimental Thermal and Fluid Science*, 29 (2005) 633-647.
[13] N. A. Ahmed and J. Goonaratne, Lift augmentation of a low-aspect-ratio thick wing in ground effect, *J. Aircraft*, 39 (2) (2002) 381-384.
[14] Arthur E. Raymond, Ground influence on airfoils, NACA TM 67 (1921).
[15] R. D. Irodov, Criteria of longitudinal stability of ekranoplan, Ucheniye Zapiski *TSAGI*, 1,(4) (1970) 63-74.
[16] Nikolai Kornev and Konstantin Matveev, Complex numerical modeling of dynamics and crashes of wing-in-ground vehicles, AIAA 2003-600, *41st Aerospace Sciences Meeting and Exhibit*, Jan., (2003), Reno, Nevada.

Dr. Juhee Lee graduated in 2006 Ph. D on "Pareto optimization of WIG airfoil based on the multi-objective genetic algorithm" from Hanyang University. Working at a CFD engineering company for 5 years as a senior engineer. A lecturer of the Hoseo University since 2007. Major topics of interest covers WIG design, aircraft performances, fluid dynamics, numerical methods, and multi-objective optimization.

Prof. Kyoungwoo Park is currently working at Hoseo University. After received his Ph. D in mechanical engineering of Hanyang University, he had worked as a senior engineer at LG Electronics for four years. And then, he had joined at IDOT(Hanyang University) and UC Berkeley as a research professor and visiting scholar, respectively. During those days, his major topics of interest extended from heat transfer to Computational Fluid Dynamics and optimzation.